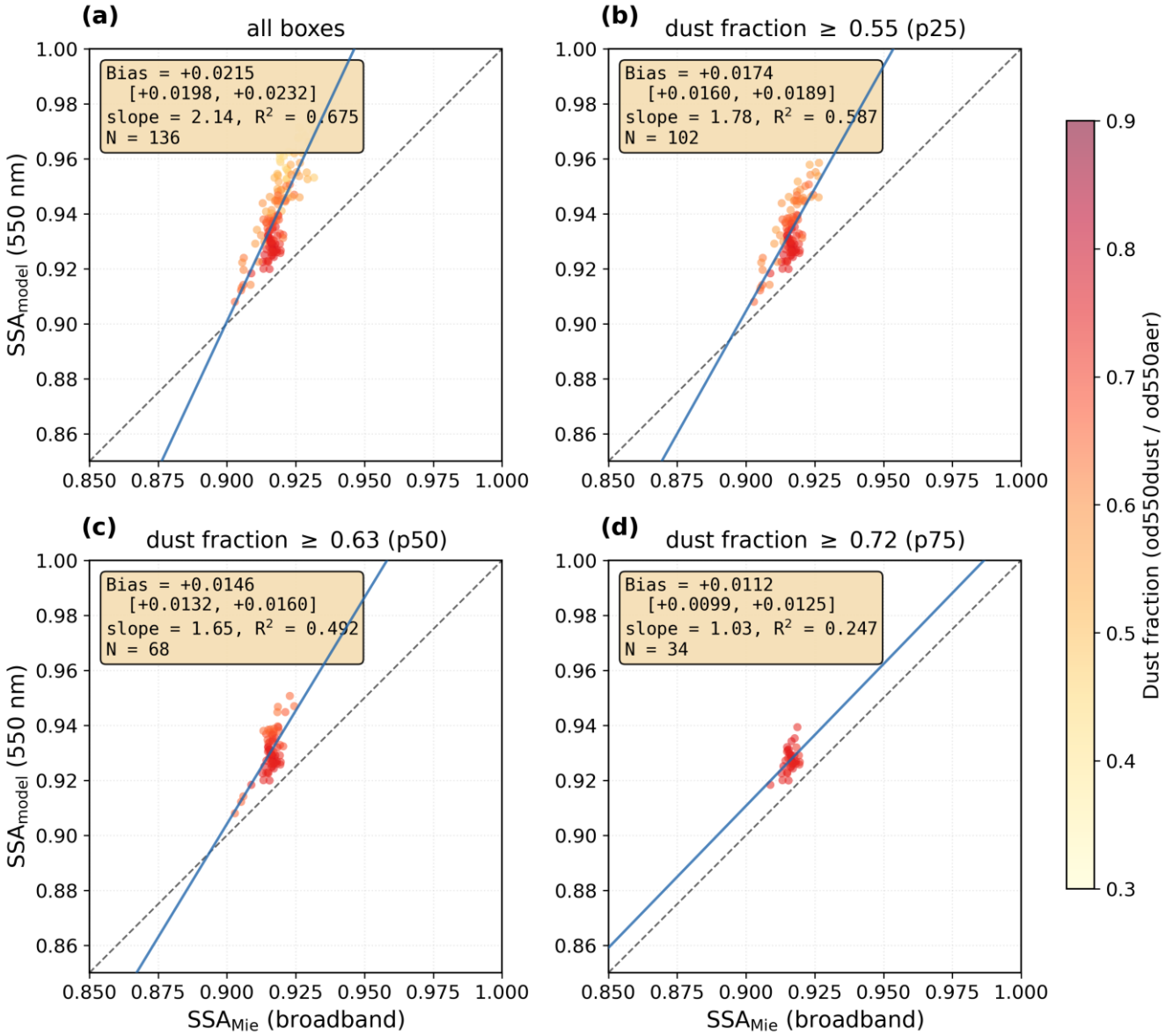


Figure S1. Internal consistency check of the Saharan SSA diagnostic in UKESM1. Mie-calculated dust SSA versus model-output aerosol SSA at 550 nm over Saharan grid boxes. Points are colored by dust fraction, defined as $\tau^{550}_{\mathrm{ext,dust}}/\ \tau^{550}_{\mathrm{ext,aer}}$. Panels show (a) all grid boxes and subsets with dust fraction greater than or equal to the (b) 25th, (c) 50th, and (d) 75th percentiles. The dashed line denotes the one-to-one relationship, and the blue line denotes the ordinary least-squares fit. Text boxes report the mean bias, 95 % confidence interval, regression slope, R^2, and sample size.

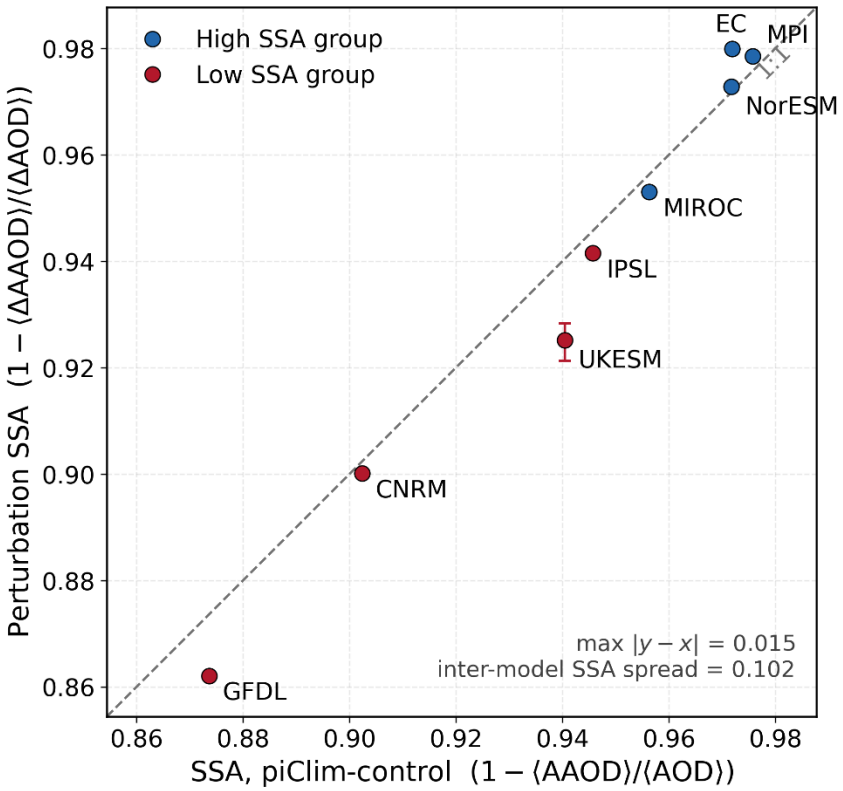


Figure S2. Consistency between the control-based and perturbation-based Saharan SSA. Control-based Saharan SSA, calculated from piClim-control as $1 - \langle AAOD \rangle / \langle AOD \rangle$, is compared with perturbation-based SSA, calculated from the dust-induced optical-depth change as $1 - \langle \Delta AAOD \rangle / \langle \Delta AOD \rangle$. The angle brackets denote averages over the Saharan land region. Blue and red markers indicate High-SSA and Low-SSA groups, respectively. The dashed line denotes the one-to-one relationship. Model labels indicate individual CMIP6 models. The maximum absolute difference between the two diagnostics and the inter-model SSA spread are shown in the lower-right corner.

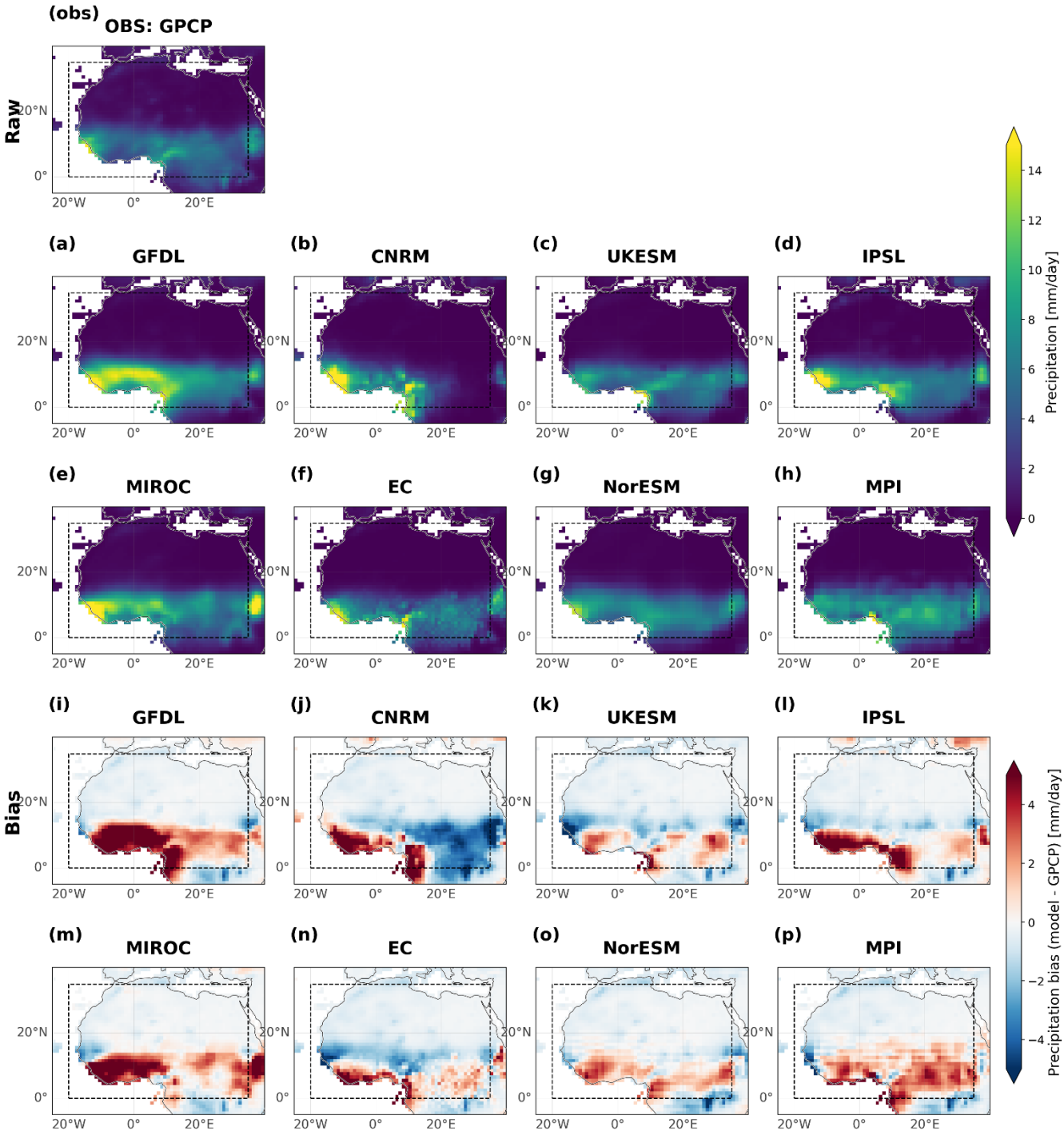


Figure S3. JJA mean precipitation over West Africa from GPCP observations for 1995–2014 and from the CMIP6 historical simulations of the eight analyzed models. The upper panels show the raw climatological mean precipitation fields, and the lower panels show the model bias relative to GPCP. The dashed boxes indicate the analysis domains used in this study.

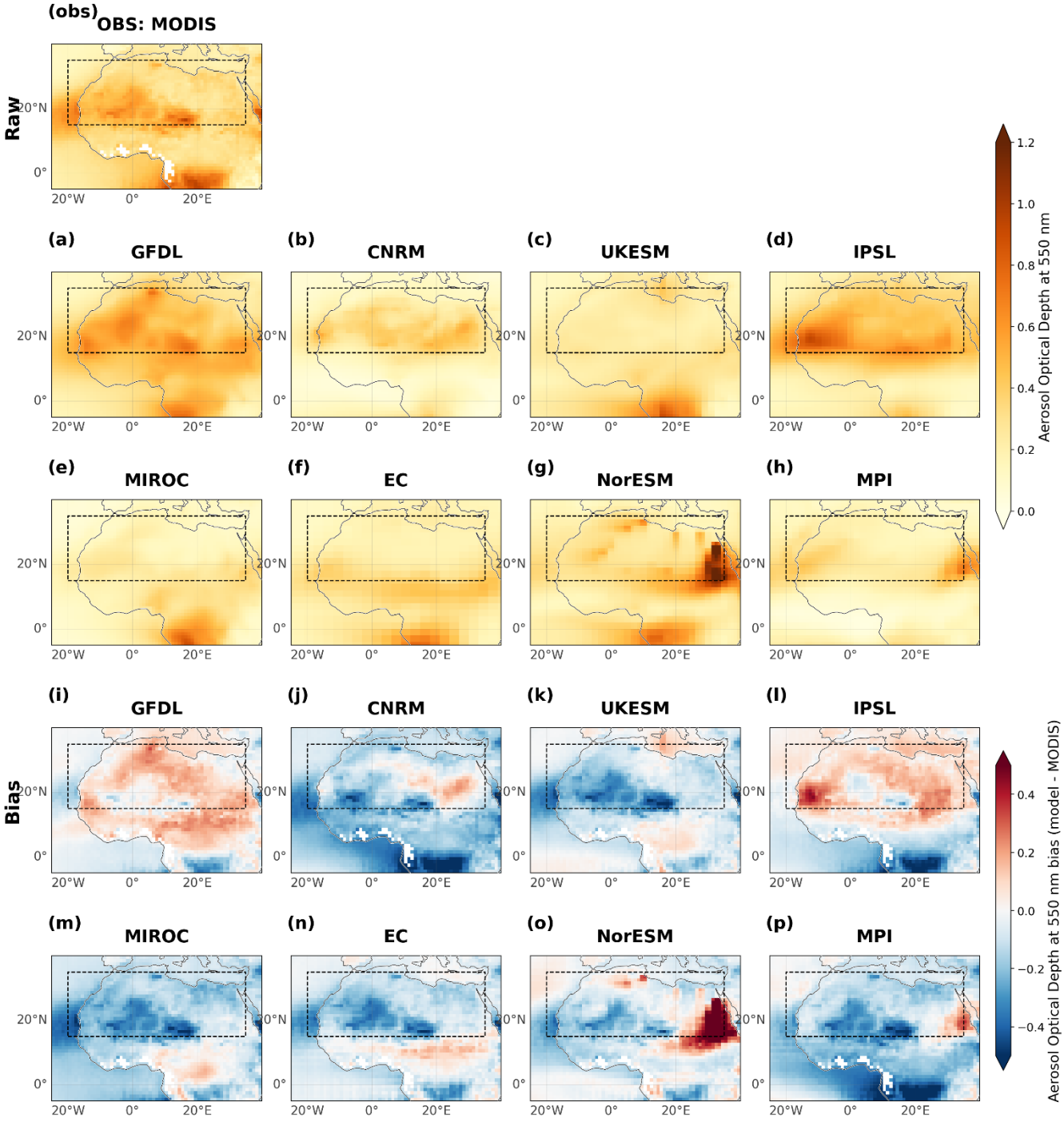


Figure S4. JJA mean AOD at 550 nm over North Africa from MODIS observations for 2003–2014 and from the CMIP6 historical simulations of the eight analyzed models. The upper panels show the raw climatological mean AOD fields, and the lower panels show the model bias relative to MODIS. The dashed boxes indicate the Sahara analysis domain used in this study.

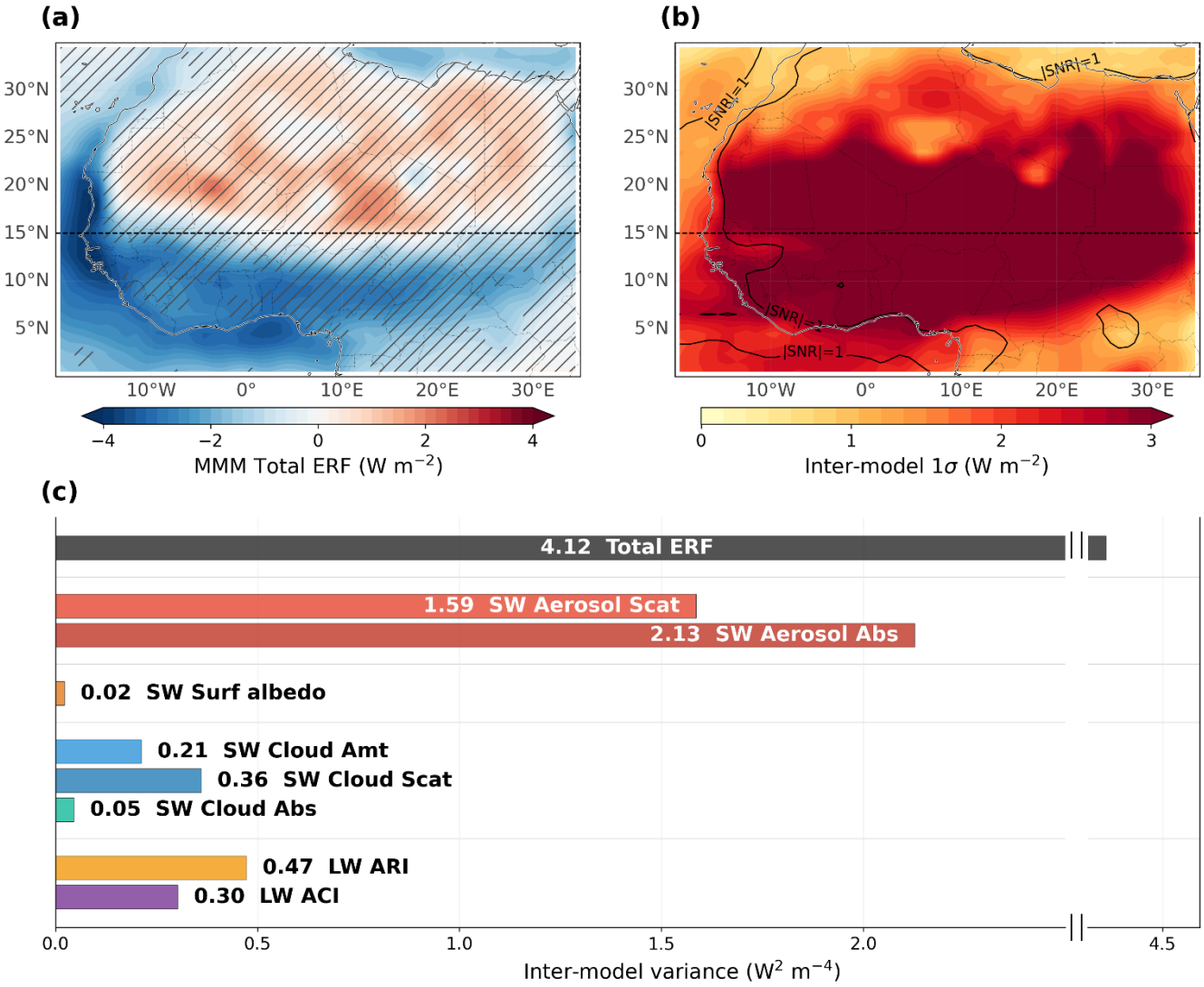


Figure S5. Inter-model spread of the total dust effective radiative forcing (ERF) over West Africa. (a) Multi-model mean total ERF (W m⁻²); hatching indicates regions where fewer than six of the eight models agree on the sign of the response. (b) Inter-model standard deviation of total ERF; black contours mark $|\mathrm{SNR}| = 1$, where the absolute value of the multi-model mean equals one inter-model standard deviation. (c) Inter-model variance of the area-mean APRP components, calculated over West African grid cells with $\Delta\,\mathrm{AOD} \geq 0.01$. The grey reference bar denotes the variance of the total ERF.

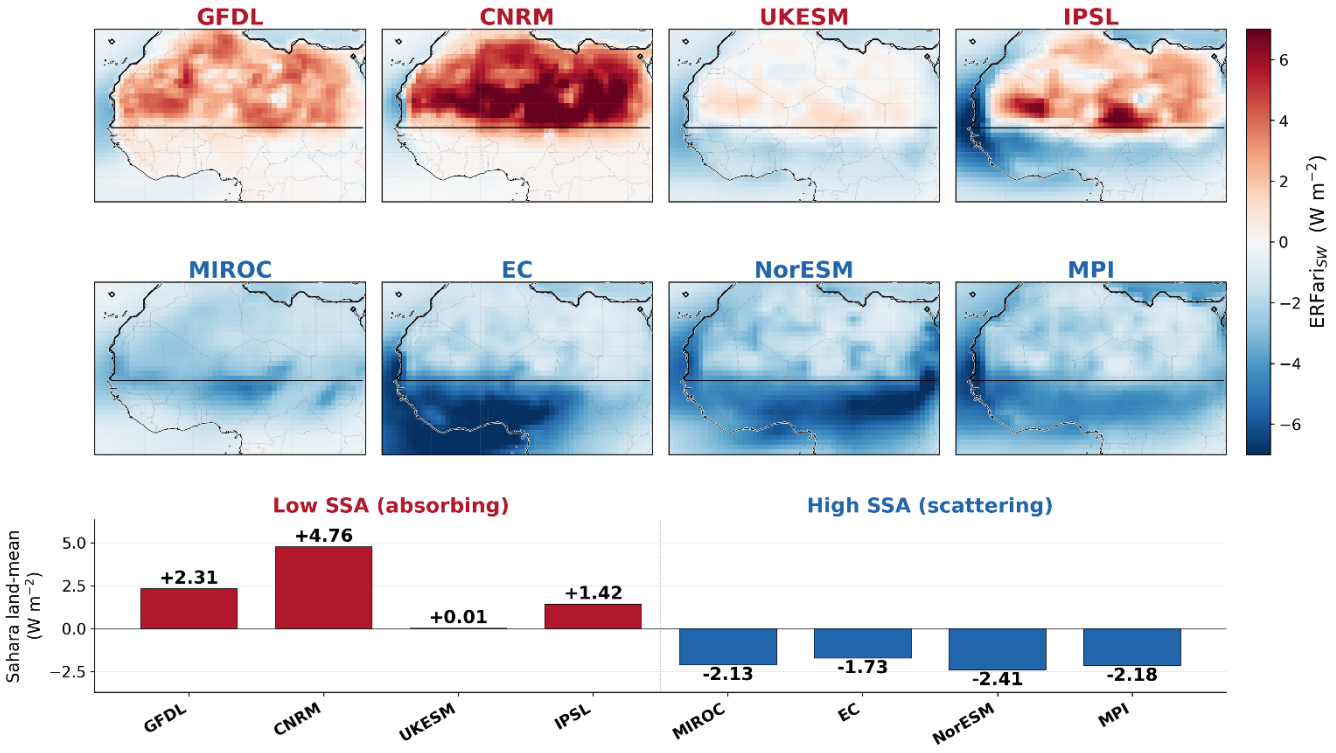


Figure S6. Model-by-model SW aerosol–radiation forcing over West Africa. (a) Annual-mean ERF_{ari}^{SW} (W m^{-2}) for piClim-2xdust minus piClim-control in each of the eight analyzed CMIP6 models. The dashed boxes indicate the Sahara region used to calculate the land-mean values. Model names are colored by SSA group, with red indicating Low-SSA, more absorbing models and blue indicating High-SSA, more scattering models. (b) Sahara land-mean ERF_{ari}^{SW} for each model. Low-SSA models generally produce near-zero to positive SW forcing over the Sahara, whereas High-SSA models produce negative SW forcing.

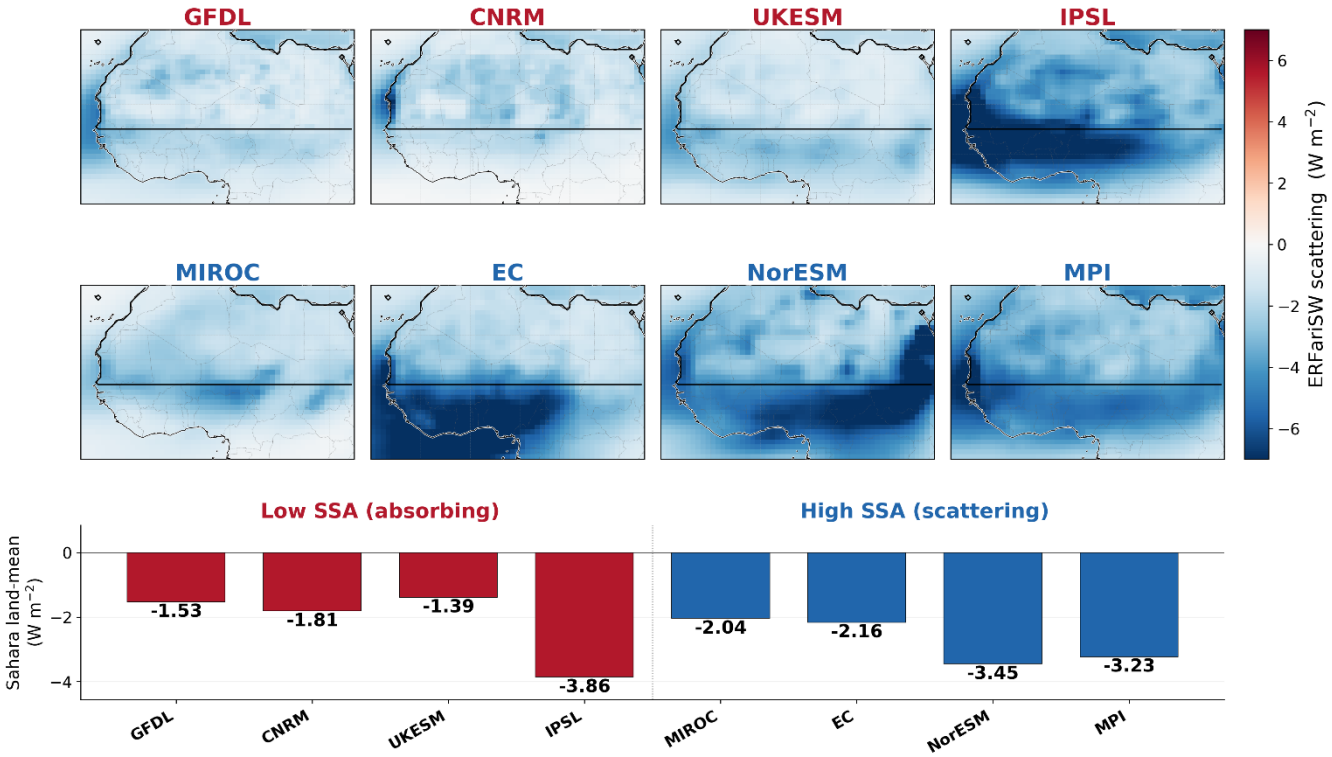
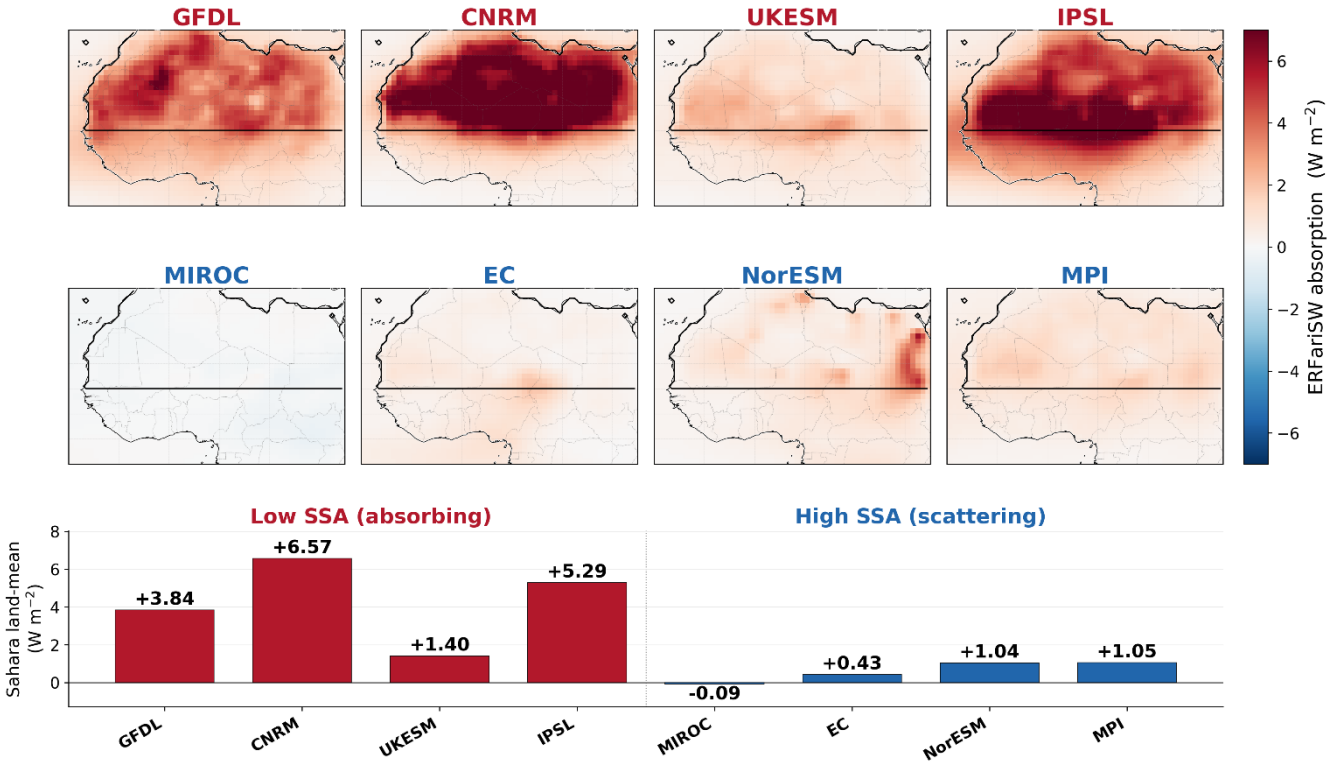


Figure S7. Same as Fig. S6, but for the SW scattering component of ERF_{ari}^{SW}.



55

56

57 **Figure S8.** Same as Fig. S6, but for the SW absorption contribution to $\mathrm{ERF}_{\mathrm{ari}}^{\mathrm{SW}}$.

58

59

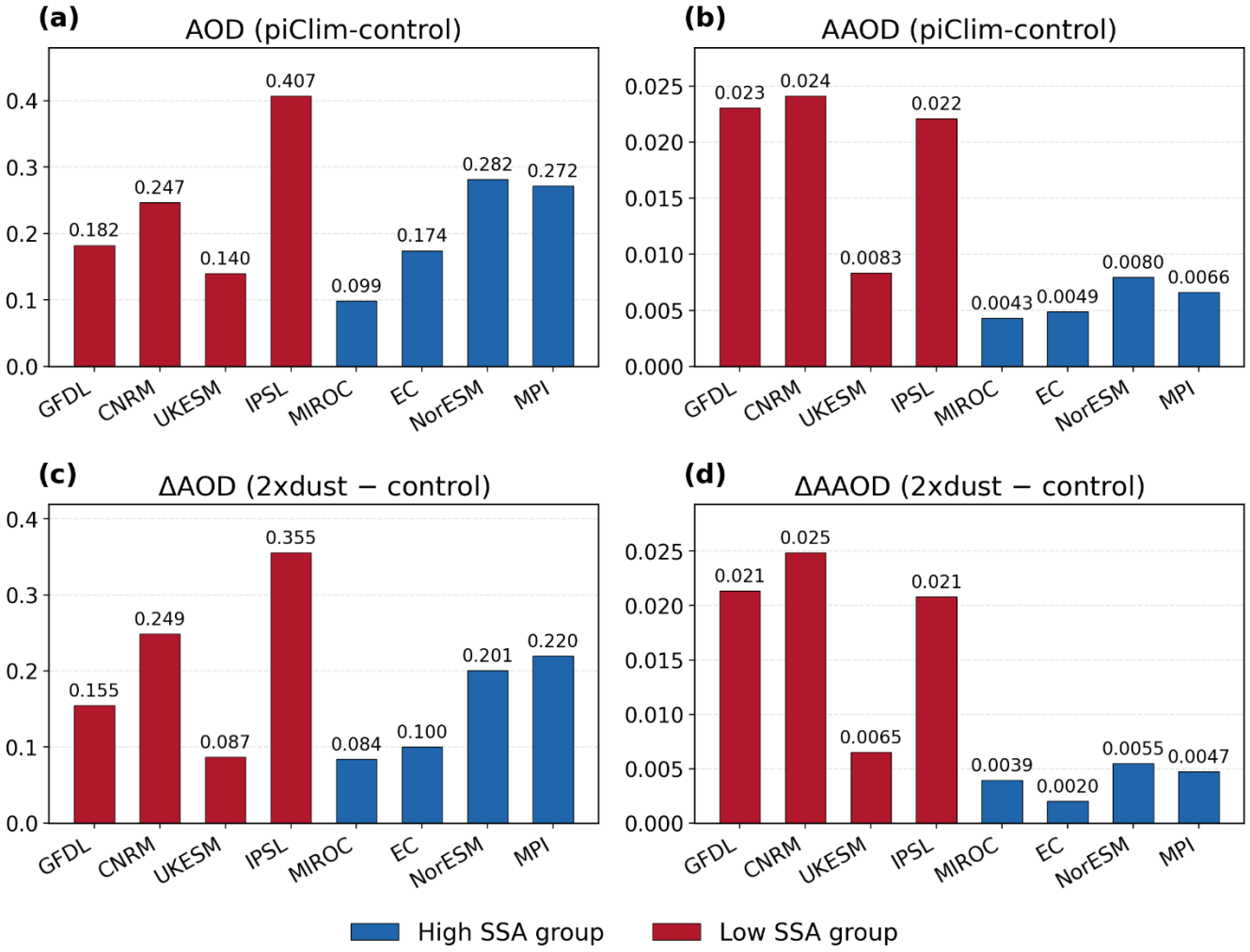


Figure S9. Sahara-mean aerosol optical properties at 550 nm for each of the eight analyzed CMIP6 models. (a) AOD ($\tau_{\mathrm{ext}}^{550}$) in piClim-control. (b) Absorption AOD (AAOD; $\tau_{\mathrm{abs}}^{550}$) in piClim-control. (c) Dust-induced change in AOD ($\Delta\tau_{\mathrm{ext}}^{550}$), defined as piClim-2xdust minus piClim-control. (d) Dust-induced change in AAOD ($\Delta\tau_{\mathrm{abs}}^{550}$), defined as piClim-2xdust minus piClim-control. Bar colors indicate the SSA grouping used in the composite analysis, with red for the Low-SSA group and blue for the High-SSA group.

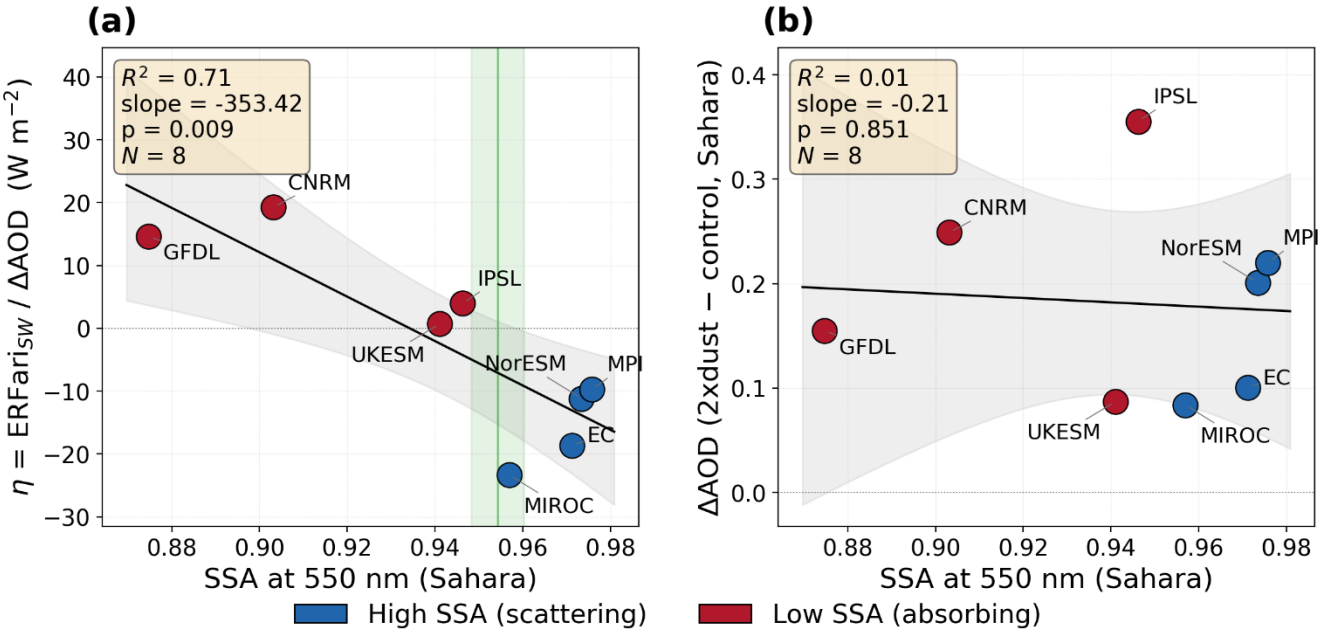


Figure S10. Relationship of Saharan column SSA with forcing efficiency and dust optical-depth perturbation. (a) Saharan SW aerosol–radiation forcing efficiency, defined as $\eta = \mathrm{ERF}_{\mathrm{ari}}^{\mathrm{SW}}/\Delta\mathrm{AOD}$, plotted against Saharan column SSA at 550 nm for each of the eight analyzed CMIP6 models. (b) Dust-induced change in Saharan AOD, $\Delta\,\mathrm{AOD}$, defined as piClim-2xdust minus piClim-control, plotted against Saharan column SSA. The green dashed line and band in (a) indicates the AERONET-based observational SSA constraint, 0.9543 ± 0.0060. Black lines in (a) and (b) show ordinary least-squares regressions, and grey shading denotes the regression uncertainty. Model colors indicate the SSA grouping, with red for Low-SSA models and blue for High-SSA models.

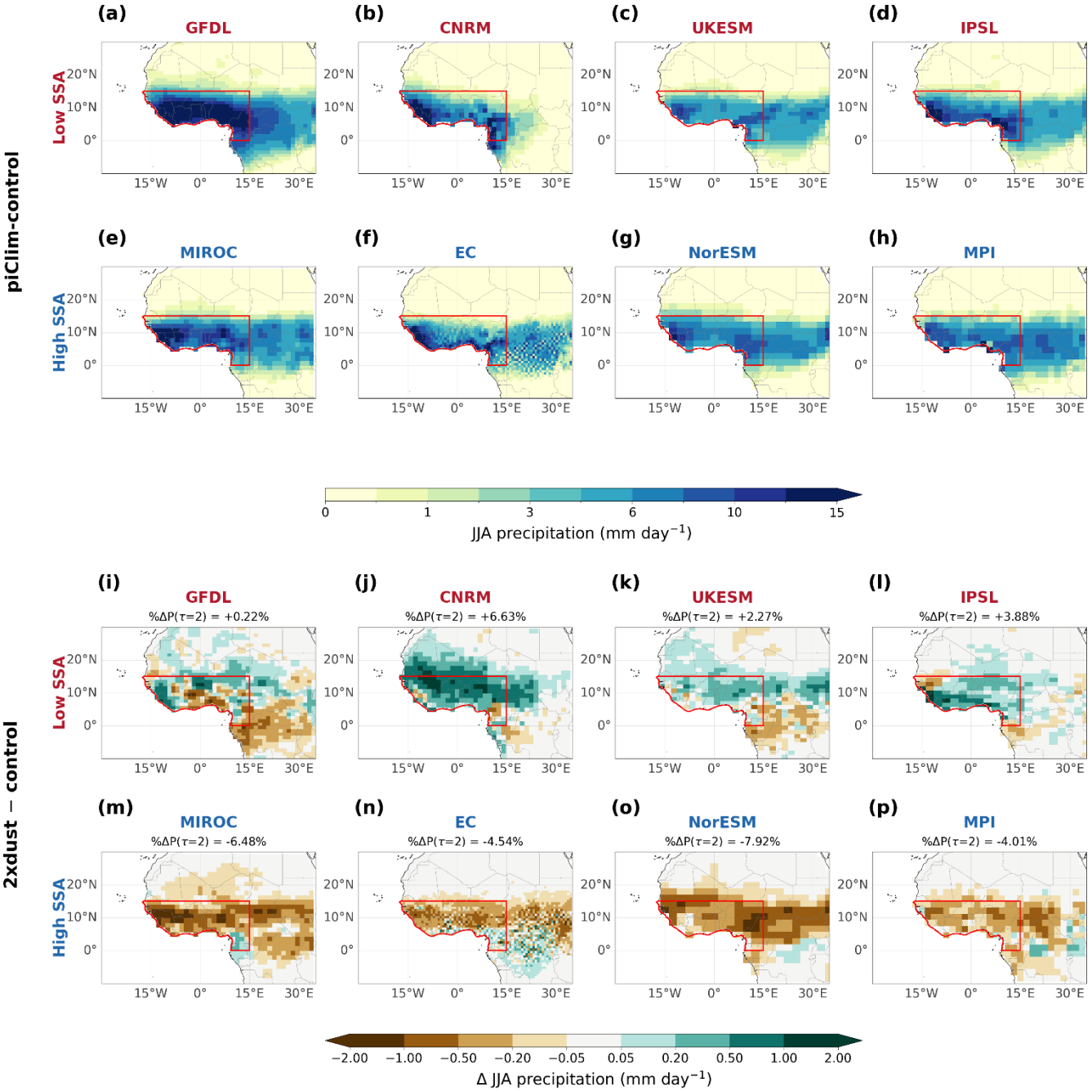


Figure S11. Model-by-model JJA precipitation climatology and response to dust-emission perturbation. The top two rows show piClim-control JJA mean precipitation over land for the eight analyzed CMIP6 models, and the bottom two rows show the corresponding precipitation response, defined as piClim-2xdust minus piClim-control. Models are ordered by Saharan SSA group, with Low-SSA models in red and High-SSA models in blue. The red outline denotes the Sahel land region used for regional diagnostics. Panel subtitles in the response maps give the fractional change in Sahel rain-band area, $\%\Delta P$, calculated using a precipitation threshold of $\tau = 2$ mm d^{-1}. Positive values indicate expansion or strengthening of the Sahel rain band, whereas negative values indicate

contraction or weakening.